Failure mechanism transition of hydrogen embrittlement in AISI 304 K-TIG weld metal under tensile loading

Xiaogang Li[a,b], Baoming Gong[a,b,*], Caiyan Deng[a,b,*], Yizhe Li[a,b]

[a] Department of Materials Science and Engineering, Tianjin University, Tianjin 300350, China
[b] Tianjin Key Laboratory of Advanced Joining Technology, Tianjin 300350, China

ARTICLE INFO

ABSTRACT

The effect of hydrogen on the tensile properties of AISI 304 K-TIG weld metal is investigated in this study. Fractographic analysis demonstrates a transition from quasi-cleavage/cleavage fracture to intergranular fracture in the brittle zone as the hydrogen-charging current density increases, which is attributed to the interplay of crystalline defect, hydrogen atoms, and α′ martensite transformation sites. It is believed that at low current density, α′ martensite nucleates and grows homogeneously in the interior of the grain. At high current density, the stress-induced α′ martensite forms preferentially at the grain boundary, which undergoes severe strain localisation and hydrogen atom segregation.

1. Introduction

Due to the its superior resistance to hydrogen embrittlement (HE), good mechanical properties, as well as outstanding performance in machining and welding [1–9], the 300-series austenitic stainless steel (ASS) is widely employed in the production, storage, and distribution of both gaseous and liquid hydrogen. The susceptibility of ASS to HE depends significantly on the stability of austenite, as widely reported in the literatures [10–12]. However, because of the phase transformation from austenite to α′ martensite during plastic deformation [13–16], metastable ASS such as the type 304 ASS often suffers from severe HE [12,17,18]. Moreover, since the hydrogen diffusion coefficient in α′ martensite (bcc) is higher than that in γ (fcc) [18–20], α′ martensite is usually more sensitive to HE than austenite. Therefore, α′ martensite in ASS is regarded as "hydrogen diffusion highway" [21–23]. HE in austenitic steel could induce slip dislocation motion [24,25], deformation twinning [26,27], and lowered grain boundary cohesive energy [28,29]. Consequently, the fracture morphology from HE can transform ductile microvoid coalescence into cleavage and even intergranular fracture modes [30,31]. Therefore, the effects of hydrogen atom diffusion on the fracture mechanism and the related austenite-to-α′ martensite phase transformation have been widely investigated in both ASS and its welding joints [7,32–36]. In the welded joints of ASS, the microstructure of weld metal is usually distinct from that of the base metal [32,35,37–39], which may affect the hydrogen transport significantly [40–44] and increase the susceptibility to HE [45–48]. However, little is known about the relationship among hydrogen atoms, crystalline

defects, and α′ martensite transformation sites in the weld metal of ASS.

Keyhole tungsten inert gas (K-TIG) welding method was introduced by the Australian Commonwealth Scientific and Industrial Research Organization (CSIRO) in 1997. In this method, a keyhole is formed inside the weld pool due to a high arc pressure and heat input [49]. Therefore, the K-TIG method can achieve deeper penetration and higher efficiency without filler in the welding of ASS compared to the classical TIG method. The primary aim of the current study is to investigate the influence of hydrogen content on the tensile failure mechanism in AISI 304 stainless steel (SS) K-TIG weld. The correlation between the microstructural and fractographic features of the weld metal is further discussed with the aid of electron backscatter diffraction (ESBD) and transmission electron microscopy (TEM). The results demonstrate that the localisation of hydrogen along the crystalline defects (i.e. grain boundary, deformation twinning, and stack fault) could cause the desired phase transformations from austenite to α′ martensite under plastic strain, which may be responsible to the transition of failure mechanism in the brittle zone from quasi-cleavage or cleavage fracture to intergranular fracture.

2. Material and methods

2.1. Materials and welding parameters

The welding process employed a K-TIG torch operated with a direct current electrode negative (straight) polarity and powered by a Miller 1250 source. The base metal was AISI 304 stainless steel plate, with a

* Corresponding authors at: Department of Materials Science and Engineering, Tianjin University, Tianjin 300350, China.
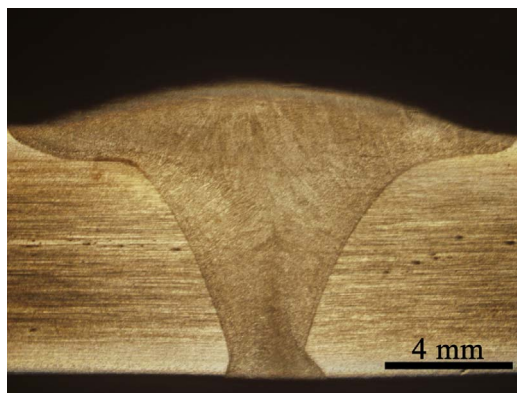 E-mail addresses: gongbm@tju.edu.cn (B. Gong), dengcy@tju.edu.cn (C. Deng).

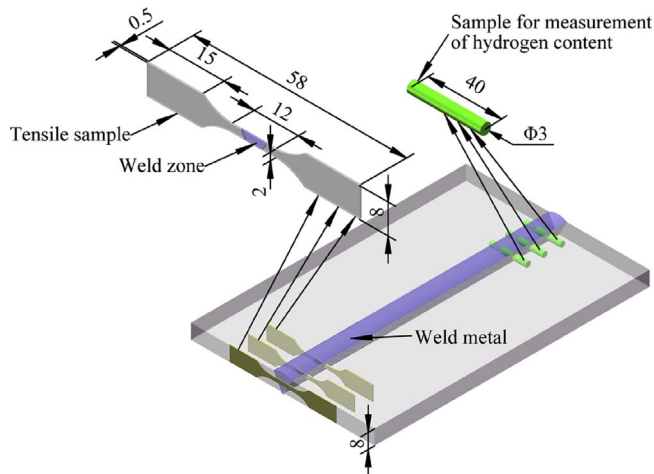**Fig. 1.** OM images of the cross section of K-TIG weld joint.

Fig. 2. Dimensions and sampling location of samples for tensile and hydrogen content measurements (in mm).

chemical composition (mass percentage) of 18.39 Cr, 8.56 Ni, 1.40 Mn, 0.40 Cu, 0.35 Mo, 0.21 Si, 0.16 Co, 0.081 N, 0.033 P, 0.024 S, and 0.019C (Fe balance). The dimensions of the plate were 300 mm × 150 mm × 8 mm. The butt-welding component was grooved and welded without filler under a current of 520 A, a voltage of 16.5 V, and at a welding speed of 6 mm/s. The shielding gas was pure argon at the flow rate of 35 L/min. The cross section of the K-TIG weld joint was chemically etched with a solution containing hydrochloric acid (30 vol%), nitric acid (30 vol%), and acetic acid (40 vol%), and then observed with an optical microscope (OM, Olympus, GX51) as shown in Fig. 1. An EBSD system (FE-SEM, JEOL, JSM-7100F) was operated at 20 kV to observe the microstructures of the K-TIG weld joint. The sample for EBSD observation was grinded down to 3000 grit, and then electro-polished with a solution containing ethyl alcohol (95 vol%) and perchloric acid (5 vol%) at 30 V for 30 s. The step size for EBSD operation was 0.1 μm, and the raw data were processed using Orientation Imaging Microscopy software (TSL-OIM). The dimensions of the tensile sample are shown in Fig. 2. The longitudinal direction is perpendicular to the welding direction. The tensile samples were grinded down to 2000 grit, then mechanically polished down to a 0.25 μm surface finish, and finally finished until reaching a thickness of 0.5 mm.

2.2. Hydrogen charging process and measurement of hydrogen content

The tensile samples were charged in a solution of H_2SO_4 (0.5 mol/L) and NH_4SCN (3 g/L) at current densities of 10, 30, 50, or 100 mA/cm^2 for 96 h. A square platinum net of 15 mm × 15 mm was used as an anode, and the samples were completely immersed during the hydrogen
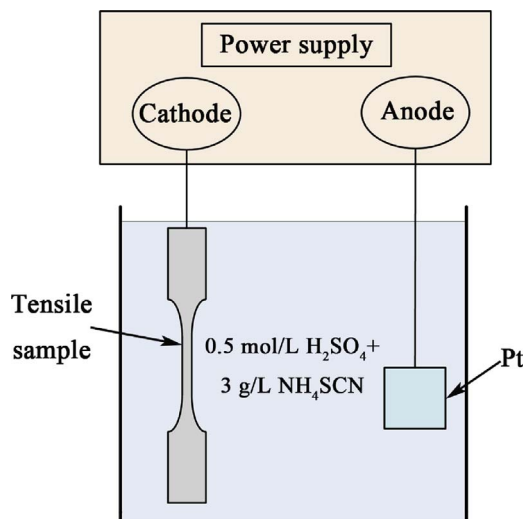

Fig. 3. Schematic of the electrolytic hydrogen charging system.

charging as shown in Fig. 3. The surface area of the sample being charged was 674 mm^2. After the hydrogen charging process, the hydrogen content in the sample was immediately determined by thermal desorption spectroscopy (TDS) analysis using a quadrupole mass spectrometer (R-DEC Company, EX0014) with a high accuracy of 0.01 wppm. The test was conducted at a heating rate of 100 °C/h in the temperature range from 25 °C to 800 °C. The dimensions of the sample for hydrogen measurement are shown in Fig. 2.

2.3. Tensile tests

After hydrogen charging, tensile tests were immediately carried out by using a micro-mechanical testing machine (Instron 5848) at room temperature and a constant displacement rate of 2 mm/min. In order to quantitatively describe the tensile ductility, two hydrogen embrittlement sensitivity indexes, I_δ and I_ψ, are calculated as follows:

$$I_\delta(\%) = \frac{\delta_0 - \delta_H}{\delta_0} \times 100\% \tag{1}$$

$$I_\psi(\%) = \frac{\psi_0 - \psi_H}{\psi_0} \times 100\% \tag{2}$$

where δ and Ψ refer to the elongation to failure and the reduction of sample area, respectively; the subscripts 0 and H denote the pristine and the charged samples, respectively.

After the tensile tests, the fracture morphologies were observed by scanning electron microscopy (SEM, Hitachi, S4800). The deformation microstructures around the necking zone of the broken samples were detected by EBSD. A field-emission transmission electron microscope (FE-TEM, JEOL, JEM-2100F) was operated at 200 kV to observe the dislocation, the stress-induced α′ martensite, and the deformation twins in the broken samples. The samples for TEM observation were prepared by twin-jet electro-chemical polishing using an electrolyte consisting of ethyl alcohol (90 vol%) and perchloric acid (10 vol%).

3. Results and discussion

3.1. Microstructure and hydrogen content

The fusion zone–heat-affected zone (FZ–HAZ) and HAZ–base metal boundaries were determined by EBSD mapping as shown in Fig. 4. The average width of the HAZ was 200 ± 20 μm, with grain size ranging from 10 to 80 μm. Fig. 4 demonstrates that the equiaxed grains in the HAZ are slightly smaller than those in the base metal, and the FZ contained a large amount of low-angle (< 5°) subgrain boundaries.